Bipolar Copolymers as Host for Electroluminescent Devices: Effects of Molecular Structure on Film Morphology and Device Performance

Biwu Ma,[†] Bumjoon J. Kim,[†] Lan Deng,[†] Daniel A. Poulsen,[†] Mark E. Thompson,[‡] and Jean M. J. Fréchet*,[†]

Materials Sciences Division, Lawrence Berkeley National Laboratory, Berkeley, California 94720, Department of Chemistry, University of California—Berkeley, Berkeley, California 94720-1460, and Department of Chemistry, University of Southern California, Los Angeles, California 90089

Received July 12, 2007; Revised Manuscript Received September 4, 2007

ABSTRACT: Bipolar transport polymers have been developed as host materials for electroluminescent devices by incorporating both electron-transporting and hole-transporting functionalities into copolymers. Two different copolymers having the same molecular weight ($M_n \sim 30$ kg/mol) and the same fraction of electron-transporting monomers ($f_{OXA} = 0.50$) have been synthesized in the form of random and diblock copolymers, respectively. The effect of molecular structure and film morphology of these bipolar polymers on device performance has been studied. For the diblock copolymers, pronounced phase segregation forming different nanomorphologies has been observed by modern microscopic techniques, which is not observed for the random counterparts under the same thin film preparation conditions. The results of single-layer polymer light emitting diodes (PLEDs) show that the nanophase separation morphology of diblock copolymers has a significant effect on device performance: lowering charge transport and facilitating the hole−electron recombination leads to a much higher quantum efficiency. Applying this high triplet block copolymer as host, a high external quantum efficiency of 5.4% at the brightness of 900 cd/m^2 was achieved for *single-layer* PLEDs with a green-emitting complex dopant.

Introduction

Organic light-emitting diodes (OLEDs) have attracted great attention due to their potential application in both flat-panel displays and lighting sources.[1−8] Identifying new materials plays a significant role in realizing high-performance OLEDs. To date, there are two major kinds of materials that have been widely applied: conducting polymers and small molecular organic materials. An advantage of the polymeric materials is related to the fact they can be solution processed, a process that has potential to lower manufacturing costs and is less time-consuming than the highly successful high vacuum vapor deposition process used with small molecules today. However, typical polymer LEDs (PLEDs) only provide fluorescence, which has limited internal quantum efficiencies of 25%, since only singlet excitons can be utilized.[4] To our best knowledge, the highest external quantum efficiency (EQE) achieved for PLEDs with fluorescent polymers as active emitting species is about 6% for white luminescence.[8] Indeed, applying phosphorescent molecules as emitting materials, such as iridium and platinum complexes, can potentially provide 100% internal quantum efficiencies.[3,5−7,9−11] This is due to the strong spin−orbital coupling of heavy metals that facilitates efficient intersystem crossing and allows complexes to capture both singlet and triplet excitons. Therefore, solution-processed, highly efficient PLEDs have been demonstrated by physically doping phosphorescent molecules in polymer matrix or chemically bonding them to polymer chains.[12−21]

However, the properties of host polymers, such as the triplet energy, the charge-transporting properties, and the balance of holes and electrons that control various aspects of device behavior, should be judiciously chosen to maximize the device performance. For example, hosts having higher triplet energy over dopants are required to avoid the energy back-transfer from the emitters to hosts that would decrease efficiency.[22] With a high triplet bipolar conjugated polymer as host, efficient PLEDs have been demonstrated with an EQE of 6.6% for green emission.[21] To achieve a good balance of holes and electrons, both hole- and electron-transporting functions should be incorporated into a single bipolar host material. In general, this has been achieved by physically blending one carrier-transporting material with the other carrier-transporting material, thus affording a bipolar host matrix. The blend of electron-transporting (2-*tert*-butylphenyl-5-biphenyl-1,3,4-oxadiazole) PBD with the hole-transporting poly(*N*-vinylcarbazole), PVK is a good example of a system that has been used to produce efficient single-layer green-light emitting diodes with an EQE of 3.5%.[12] Since the photophysical and electrical behavior of polymer films is highly sensitive to aggregation and film morphology,[23−33] it is critical to control the phase-separated morphology of their blend if two immiscible polymers are used. However, this is difficult to achieve,[23] since the devices require a fine dispersion of one polymer in the other without macrophase separation. Ideally, we target a bicontinuous morphology with 10−20 nm length scale for charge transport and exciton diffusion, since it has been shown to improve the device performance in photovoltaic devices. Such a morphology, which can be obtained in a kinetically trapped nonequilibrium method, is very difficult to control and it may only be achievable in an extremely narrow regime of blend composition.[34−36] In contrast to this, a device consisting of random or diblock copolymers does not experience macrophase separation at larger than the micrometer length scale, and devices based on diblock copolymers with morphologies on the nanometer length scale can be achieved even under equilibrium.[23,37,38] Last, very little work has been done in high-triplet host polymers, especially bipolar copolymer systems.

* Corresponding author. Fax: (510) 643-3079. E-mail: Frechet@berkeley.edu.

[†] Lawrence Berkeley National Laboratory and University of California—Berkeley.

[‡] University of Southern California.

10.1021/ma0715526 CCC: $37.00
Published on Web 10/18/2007

Scheme 1. Chemical Structures of the Bipolar Copolymers ($m/n = 1$) and of the Two Phosphorescent Heavy Metal Complexes

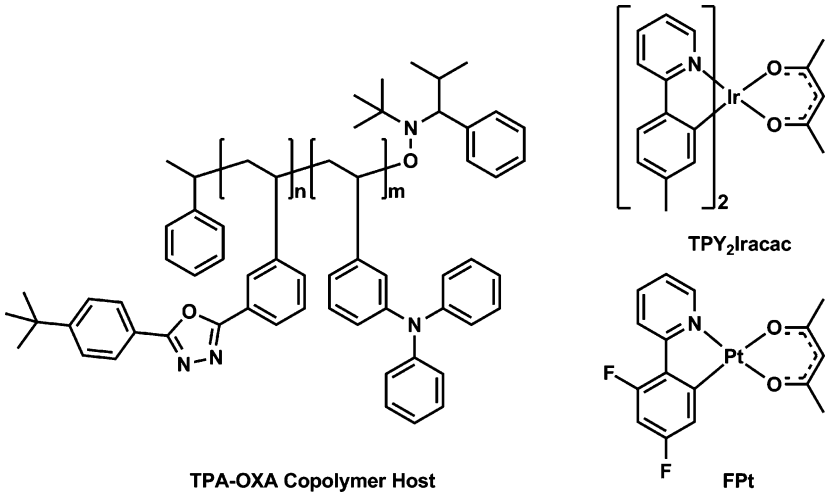

On the basis of recent developments in living radical polymerization,[39−42] we have prepared novel bipolar transport copolymers incorporating both electron-transporting and hole-transporting functionalities for use as host materials for electroluminescent devices. We demonstrate that the molecular structure of these copolymers affects the film morphology and subsequently the device performance. For films of the block copolymers, pronounced phase segregation with nanometer length scale has been observed, contrasting with the homogeneous morphology obtained for films of random copolymer with the same composition prepared under the same conditions. We find that the large interfacial area between electron- and hole-transporting domains in the block copolymer device has a dramatic influence on both charge transport and recombination. Therefore, the interfaces present in block copolymer domains facilitate recombination of holes and electrons, leading to a much higher quantum efficiency than achievable with a random copolymer, while lowering the charge transport at the same time. With optimization, high performance *single-layer* electroluminescent devices with external quantum efficiency reaching 5.6% were achieved. The high performance of these devices can be attributed to the domain separation that mimics a multilayer structure in a single-layer device, where hole-transporting and electron-transporting moieties self-assemble, forming a large interfacial area, favoring charge recombination.

Experimental Section

Materials and Film Characterization. The TPA−OXA copolymers studied in this paper were synthesized by living radical polymerization as random or block copolymers with a constant ratio of the two species: TPA/OXA = 1.[19] Heavy metal complexes were prepared as reported in the literature.[10,11] DSC was performed with a TA DSC Q200. The morphology of bulk samples as well as that of thin films of the block copolymers (B-TPA−OXA) and the random copolymers (R-TPA−OXA) was investigated by transmission electron microscopy (TEM) and atomic force microscopy (AFM). The B-TPA−OXA copolymer was annealed at 225 °C for 3 days and then at 185 °C for 1 day and cooled slowly to room temperature under vacuum. The bulk sample was microtomed into 50 nm thick film slices and sequentially stained by RuO_4 0.5% aqueous solution for 25 min, affording visual contrast between the TPA and OXA blocks. Samples for morphological study of thin film were prepared under conditions identical to those used for the devices. The films were prepared by spin-casting from chlorobenzene (40 mg mL^{-1}) onto NaCl substrate followed by transfer to the TEM grid by flotation on water. The samples were stained by RuO_4 0.5% aqueous solution for 25 min. The morphology of cross-sectioned bulk and thin film samples was observed using a FEI Tecnai operated at 200 kV. A multimode AFM (Veeco) was used in a tapping mode to investigate the two-dimensional surface topology of the T-TPA−OXA and R-TPA−OXA films on ITO/glass substrate as used for device fabrication.

Devices Fabrication and Measurement. Prior to device fabrication, substrates with ITO on glass were patterned as 2 mm wide stripes with resistivity of 20 Ω/sq. The substrates were cleaned by sonication in a soap solution; rinsed with deionized water; boiled in trichloroethylene, acetone, and ethanol for 5 min each; and then blown dry under a stream of nitrogen gas. Finally, the substrates were treated with UV/ozone for 10 min. The organic active layer was prepared by spin-casting solutions at 3000 rpm for 60 s. The solutions were filtered using 0.2 μm poly(vinylidene difluoride) filters prior to use. The thickness of the organic layer was monitored by ellipsometry. After spin-casting, a shadow mask with a 2 mm wide stripe was placed onto the substrates perpendicular to the ITO stripes. A cathode consisting of 1 nm thick LiF and 100 nm thick aluminum was then deposited at a rate of 0.2 and 4−5 Å/s, respectively. OLEDs were formed at the 2 × 2 mm squares where the ITO (anode) and Al (cathode) stripes intersect.

The devices were tested in air within 2 h of fabrication. The electrical and optical intensity characteristics of the devices were measured with a Keithly 2400 sourcemeter/2000 multimeter coupled to a Newport 1835-C optical meter, equipped with a UV-818 Si photodetector. Only light emitted from the front face of the device was collected and used in subsequent efficiency calculations. The electroluminescence (EL) spectra were measured on a PTI QuantaMaster model C-60SE spectrofluorimeter equipped with a 928 PMT detector and corrected for detector response. The emission was found to be uniform throughout the area of each device.

Results and Discussion

Two copolymers containing hole-transporting (HT) triphenylamine (TPA) and electron-transporting (ET) oxadiazole (OXA) functionalities ($m/n = 1$) were synthesized as shown in Scheme 1. One is a random copolymer (R-TPA−OXA) having a molecular weight M_n = 29 kg/mol and a polydispersity (PDI) = 1.15, and the other is a diblock copolymer (B-TPA−OXA) with M_n = 30 kg/mol and PDI = 1.25. The synthesis of similar copolymers has been previously reported.[19] Analysis of these polymers by differential scanning calorimetry (DSC) is shown in Figure 1. Only one glass transition temperature (T_g) at 143 °C is observed for the random copolymer (R-TPA−OXA), while two separate T_g at 131 and 168 °C are observed for the diblock copolymer (B-TPA−OXA). These two glass transitions occur at roughly the same temperature as in homopolymers of each block, $T_g \sim 125$ °C for the TPA homopolymer and $T_g \sim 182$ °C

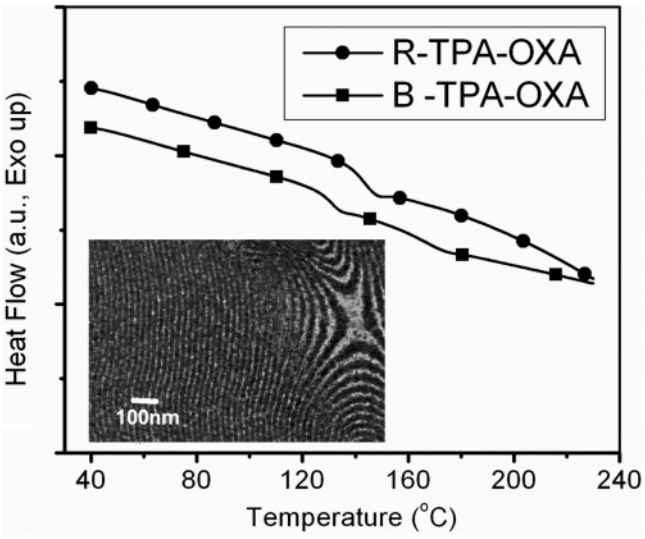

Figure 1. DSC of the two copolymers, R-TPA−OXA and B-TPA−OXA, and a TEM image of a thermally treated block copolymer bulk sample showing its lamellar structure.

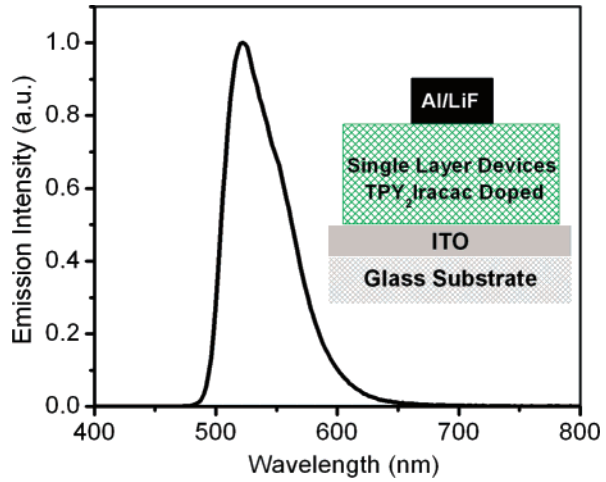

Figure 2. Electroluminescence spectrum for the device with structure of ITO/copolymers and 8 wt % TPY_2Iracac dopant (90 nm)/LiF (1 nm)/Al (100 nm).

for the OXA homopolymer. Equilibrium thin film morphologies of these copolymers were obtained by thermal annealing at 225 °C for 3 days and then at 185 °C for 1 day. The TEM image in the inset of Figure 1 shows the lamellar structure of B-TPA−OXA polymers with a domain spacing of 24 nm. The hole-transporting (TPA) and electron-transporting (OXA) components of the block copolymer self-assembled to form a clearly layered structure. In contrast, such phase separation was not observed for the random copolymer R-TPA−OXA.

We used these two HT/ET bipolar copolymers as host matrices for phosphorescent dopants in polymer LEDs to investigate the effects of the polymer composition of these polymers on device performance. Single-layer polymer LEDs were fabricated from chloroform solutions of each copolymer doped with 8 wt % green-emitting TPY_2Iracac. A 90 nm thick polymer layer was produced by spin-casting the solution on pretreated indium−tin oxide (ITO)-coated glass substrate, and metal cathodes consisting of 1 nm LiF and 100 nm of Al were vapor deposited in high vacuum chamber at lower than 3-4 × 10^{-6} Torr to give the device structure shown in Figure 2. The electroluminescent spectrum of these single-layer green phosphorescent devices in Figure 2 shows emission purely from TPY_2Iracac and the absence of either TPA or OXA emission.

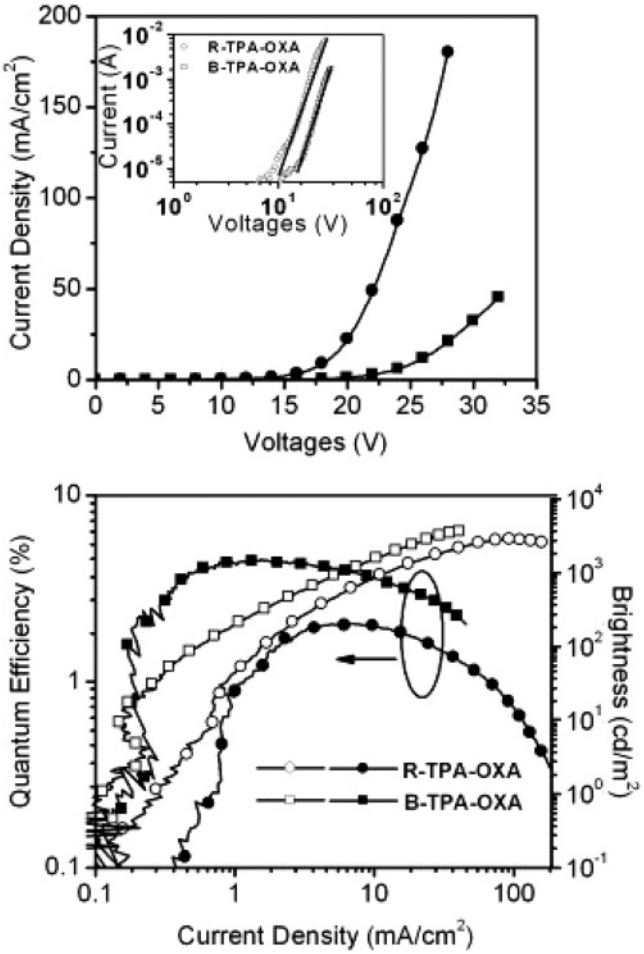

Figure 3. *I*−*V* characteristics (inset: log I-log V plots) (top), brightness vs current density and external quantum efficiency vs current density (bottom) for single-layer light-emitting diodes using TPY_2Iracac as guest and copolymers as host spin-cast from chloroform solutions: R-TPA−OXA (circles) and B-TPA−OXA (squares).

This indicates that the excitons are exclusively localized on the phosphorescent dopants prior to relaxation. Efficient energy transfer from the polymer host to the dopant is not surprising, since the triplet energy of the host (>2.5 eV) is higher than that of the dopant (2.36 eV). Figure 3 shows the device characteristics of these two different devices, and Table 1 summarizes the device performance. It was found that the R-TPA−OXA device has about 1 order magnitude higher current density over B-TPA−OXA device at the same voltage. A similar slope (∼2) was found for the log *I*−log *V* plots of the two devices in the high-voltage region, which indicates that the transport characteristics in both devices can be described using space-charge limited current (SCLC) theory in the presence of traps.[43,44] The charge transport is described by $j = 9/8\epsilon\mu_{\text{eff}}V^2/d^3$, or $I \propto V^2$, where ϵ is the permittivity of the polymer, d is the polymer film thickness, μ_{eff} is the effective mobility, and V is the applied voltage. These two devices not only exhibited different *I*−*V* characteristics but also a significant difference in quantum efficiency. As shown in Figure 3, 2−3 times higher light output was obtained from the B-TPA−OXA device than the R-TPA−OXA device operated at the same current density. The maximum external quantum efficiencies measured were $\eta_{\max} = 4.6\%$ (2.94 lm/W, achieved at 220 cd m^{-2}) for the block copolymer and 2.0% (1.5 lm/W, achieved at 560 cd m^{-2}) for the random copolymer (see Figure 3). Since the polymer chemical compositions, the dopants, and the film thicknesses are identical for both devices, we believe that the

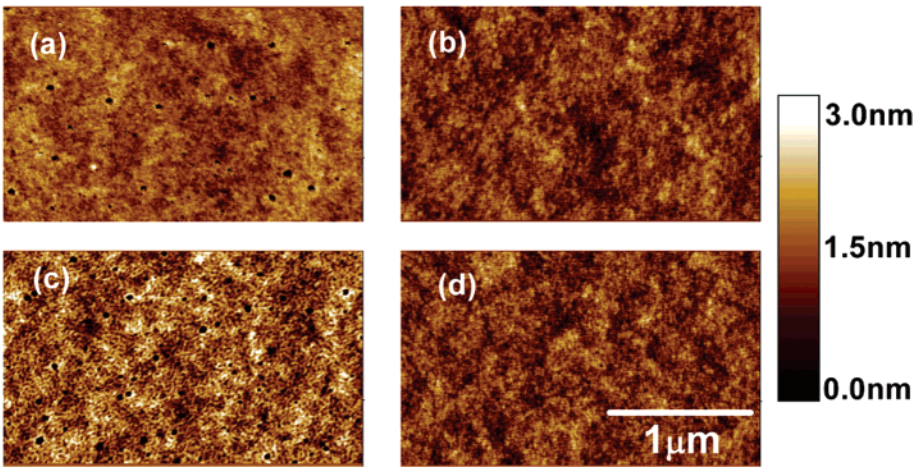

Figure 4. Tapping-mode AFM topographic images of thin films: (a) R-TPA−OXA spin-cast from chloroform, (b) R-TPA−OXA from chlorobenzene, (c) B-TPA−OXA from chloroform, and (d) B-TPA−OXA from chlorobenzene.

Table 1. Summary of Devices' Performance for Single-Layer Light-Emitting Diodes Using TPY_2Iracac as Guest and Copolymers as Host

single layer devices at ∼95 nm	random copolymer R-TPA−OXA		block copolymer B-TPA−OXA	
solvent[a]	chloroform	chlorobenzene	chloroform	chlorobenzene
turn-on voltages (V) (0.1 cd m^{-2})	7.9	5.6	8.4	5.6
maximum EQE (%)/brightness (cd m^{-2})	2.0/560	3.9/600	4.6/220	5.4/900
maximum brightness (cd m^{-2})/voltage (V)	2850/24.8	4500/23	3800/32.8	4500/25.5
EQE (%) at 800 cd m^{-2}	2.0	3.9	4.0	5.3

[a] The devices were fabricated from chloroform and chlorobenzene solutions.

dramatic difference in device performance can be attributed mainly to the film morphology, which determines the effective carrier mobility and the carrier recombination.

The difference in morphology for spun-cast thin films was investigated by AFM and TEM. Since the properties of spun-cast films are influenced by a number of factors, including solvent properties, solvent−polymer interactions, and spin-coating conditions (speed, temperature, time, etc.), we fabricated thin films using both copolymers under the same conditions to evaluate the effects of molecular structure on film architectures. Figure 4a,c represents the AFM phase images of the surface morphology for thin films obtained by spin-coating chloroform solutions of R-TPA−OXA and B-TPA−OXA. For random copolymers, the AFM phase image is smooth and featureless, suggesting a homogeneous morphology without any phase segregation of hole- and electron-transporting materials. In contrast, two distinct phases are observed in the morphology of the block copolymers. The length scale of phase separation ranges from 20 to 30 nm. AFM images of samples from chlorobenzene solutions in Figure 4b,d show improved film quality with no pinholes and a smaller root-mean-square (rms) surface roughness of 0.3 nm, as compared to chloroform samples with rms surface roughness of 0.5 nm. This can be attributed to the slower evaporation of the higher boiling chlorobenzene during film formation. Doping small molecular emitters into the two copolymers at a level of 8 wt % did not change their film morphologies. Figure 5 shows the TEM images of two copolymers containing 8 wt % of TPY_2Iracac dopant spin-coated from chlorobenzene solutions. The formation of interfaces by nanophase separation is again seen very clearly for the block copolymers but does not occur with the random copolymers. Since the movement of charge through a film occurs via a hopping process that is related to the intermolecular overlap of neighboring molecules,[33] the charge-transport behavior in both copolymers can then be described schematically, as shown in Figure 5. In the random copolymer host, holes and electrons can transport continuously in the TPA phase (HOMO orbital) and in the OXA phase (LUMO orbital), respectively, when the traps are filled at high driving voltage. However, the formation of phase-segregated domains in the B-TPA−OXA polymer device interrupts carrier-transport pathways, leading to less charge transport at the same driving voltage. Such film morphology produces a large effective interfacial area between the two domains of hole- and electron-transporting materials, facilitating recombination of opposite charges, as shown in Figure 5. This may be seen in the device characteristics reproduced in Figure 3, showing a higher light output from the block copolymer device than from the random copolymer device at the same current density. As a result of both increased charge recombination and higher operation voltage, the maximum luminous efficiency for block copolymer devices (2.94 lm/W) is about twice that of random copolymer devices (1.5 lm/W), which is less than the ratio of EQEs (4.6%/2.0% = 2.3).

Since device performance is clearly related to thin film properties and these, in turn, are affected by device fabrication conditions, we explored the use of a different organic solvent as well as different device thicknesses. Chlorobenzene was used to enhance the film quality of devices by allowing more time for the film to self-organize during the spin-casting process. Because the simple structure of a single-layer polymer LED provides no barrier for either carrier or exciton confinement within the organic layer, quenching mechanisms involving carrier leakage and/or charge trapping near the electrodes limit device performance. Therefore, shifting the recombination zone away from the electrodes and decreasing electrode quenching should improve the device quantum efficiency. Three devices using B-TPA−OXA as host were fabricated with thicknesses increasing from 71 to 95 to 125 nm, which correspond to the thickness of three, four, and five layers of TPA−OXA lamellae. Another device 95 nm in thickness was also fabricated from R-TPA−OXA for comparison purposes. As shown in Figure 6, the device made using B-TPA−OXA as the host has a higher quantum efficiency than a device with the same thickness made from R-TPA−OXA, consistent our previous observations for

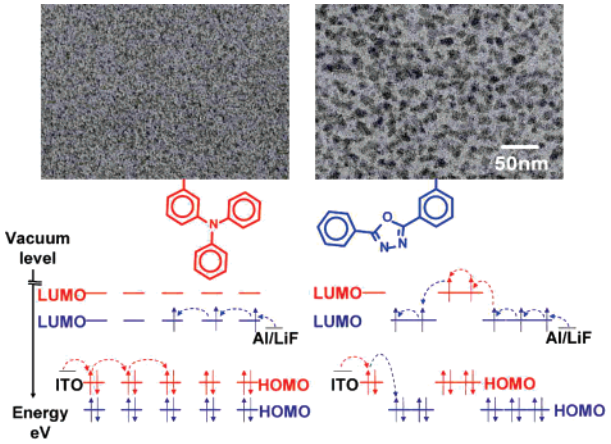

Figure 5. TEM images of thin films of R-TPA−OXA (left) and B-TPA−OXA (right) spin-cast from chlorobenzene solutions, and proposed schematic representations of charge transport for the random and block copolymers.

devices prepared from chloroform solutions. Increasing device thickness for B-TPA−OXA devices leads to a decrease in current density and increases in both turn-on voltage and external quantum efficiency. The thicker device has a larger overall interfacial area between block copolymer domains, facilitating charge recombination and affording a higher quantum efficiency. However, the use of a thicker device with its concomitant reduction in current density may also lower the probability of charge recombination away from the electrode. Therefore, an optimal thickness was found to be 95 nm for a B-TPA−OXA device, which corresponds to four layers of TPA−OXA domains. Although the highest quantum efficiency of 5.6% was measured with a device 125 nm thick, the 95 nm B-TPA−OXA with $\eta_{max} = 5.4\%$ was in fact the best device when other device characteristics, including turn-on voltage, brightness, and power efficiency, are considered. It is interesting to find that a 71 nm device of B-TPA−OXA displays a quantum efficiency performance that is similar to that of a 95 nm device of R-TPA−OXA. This is related to the more efficient carrier recombination and higher electrode/polymer interface quenching in the B-TPA−OXA device. From plots of quantum efficiency vs current density, we found that curves for block copolymer devices have a more pronounced rolling off feature than that for random copolymer devices, indicating more triplet−triplet annihilation in the former.[45]

To investigate interaction of the dopants within each of the copolymers, we fabricated single-layer devices having the following structure: ITO/8 wt % FPt-doped copolymers/LiF/Al. The platinum complex FPt was chosen as the dopant due to its pronounced molecular-aggregation-dependent red-shifted emission.[5,6,11,46] Electroluminescent spectra and external quantum efficiencies as a function of current density for these two devices are shown in Figure 7. As was the case for the iridium-doped polymer devices (Figure 3), the B-TPA−OXA device had a higher quantum efficiency than the R-TPA−OXA device. The electroluminescent spectrum of the Pt-doped block copolymer features a large platinum dimer/excimer emission peak at 600 nm, which is not seen for a device prepared using the Pt-doped random copolymer. This suggests that aggregation of FPt is favored in the environment provided by the block copolymer. This is likely due to the immiscible nature of the polymer blocks forming separate coexisting phases, which facilitates the aggregation of small molecules at the interfaces. Since device performance usually drops upon dopant aggregation, we believe that the quantum efficiency can be further improved by

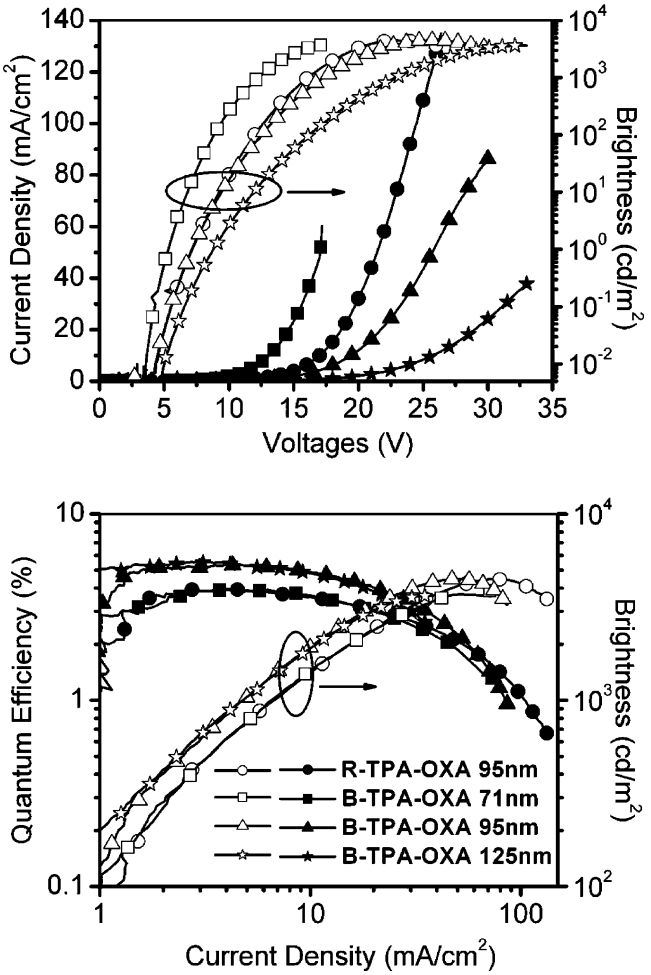

Figure 6. *I*−*V* characteristics and brightness vs voltages (top), and brightness vs current density and external quantum efficiency vs current density (bottom) for single-layer light-emitting diodes using $TPY_2Iracac$ as guest and copolymers as host spin-cast from chlorobenzene solutions in different thickness: R-TPA−OXA 95 nm (circles), B-TPA−OXA 71 nm (squares), B-TPA−OXA 95 nm (triangles) and B-TPA−OXA 125 nm (stars).

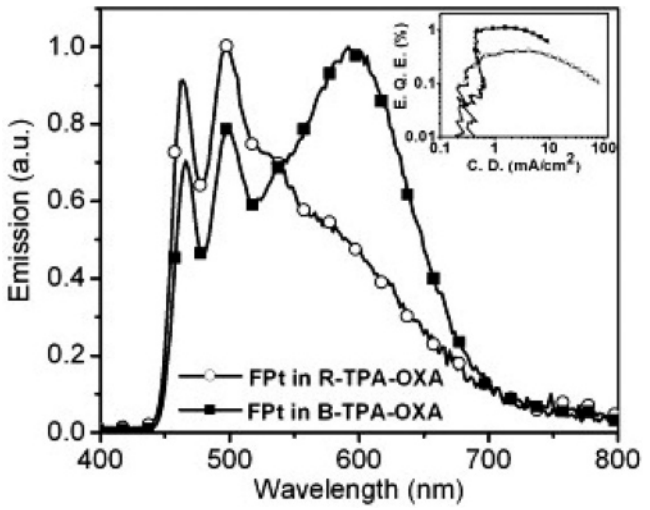

Figure 7. Electroluminescence spectra and external quantum efficiency vs current density (inset) for 8 wt % FPt-doped single-layer polymer LEDs using R-TPA−OXA and B-TPA−OXA copolymers as hosts.

dispersing the small molecules more uniformly in bipolar hosts. To achieve this, we are currently investigating three-component polymers with covalently bonded phosphorescent emitters, in which the emitting species are "doped" inside of the block

domains, not in the interfaces, leading to less aggregation. Other ways to improve the device performance will include altering the components of the charge-transporting units, altering the block sizes to reduce the phosphor aggregation, applying multilayer device structure, and so on.

Conclusion

In conclusion, we have presented a series of experiments studying the effect of molecular structure of bipolar copolymers on the film morphology and device performance. Nonconjugated copolymers containing hole-transporting and electron-transporting components were studied in random and block copolymer compositions. The morphology of B-TPA−OXA and R-TPA−OXA copolymers prepared in different solvents and thicknesses were characterized by AFM and TEM, showing phase-segregated TPA and OXA domains only in the B-TPA−OXA film. This difference in thin film morphology had a pronounced effect on electroluminescent device performance. Charge transport in the block copolymer was 1 order of magnitude lower than in the random copolymer, resulting from the domain phase separation making transport pathways through the device more circuitous. Consequently, the hole/electron recombination is enhanced by a factor of 2−3 for the block copolymer over the random copolymer, leading to a much higher quantum efficiency for *single-layer* polymer light-emitting diodes. An external quantum efficiency of 5.6% for a single-layer green electroluminescence was obtained using TPY_2Iracac as the guest and B-TPA−OXA copolymer as host. However, the self-organization of block copolymer also increased the aggregation of small molecular dopants, leading to increased triplet−triplet annihilation in polymer/dopant phosphorescent devices. Further investigation of three-component polymers with covalently bonded phosphorescent emitters is underway.

Acknowledgment. This work was supported by the Director, Office of Science, Office of Basic Energy Sciences, Division of Materials Sciences and Engineering, of the U.S. Department of Energy under Contract No. DE-AC03-76SF00098. We also thank the National Technology Laboratory of the U.S. Department of Energy under Contract No. DE-FC26-04NT42272 for the support of testing facilities at USC. The authors acknowledge support of the National Center for Electron Microscopy, Lawrence Berkeley Lab, which is supported by the U.S. Department of Energy under Contract No. DE-AC02-05CH11231 for sample preparation of TEM.

References and Notes

(1) Tang, C. W.; VanSlyke, S. A. *Appl. Phys. Lett.* **1987**, *51*, 913−915.
(2) Brown, A. R.; Bradley, D. D. C.; Burroughes, J. H.; Friend, R. H.; Greenham, N. C.; Burn, P. L.; Holmes, A. B.; Kraft, A. *Appl. Phys. Lett.* **1992**, *61*, 2793−5.
(3) O'Brien, D. F.; Baldo, M. A.; Thompson, M. E.; Forrest, S. R. *Appl. Phys. Lett.* **1999**, *74*, 442−444.
(4) Friend, R. H.; Gymer, R. W.; Holmes, A. B.; Burroughes, J. H.; Marks, R. N.; Taliani, C.; Bradley, D. D. C.; Dos Santos, D. A.; Bredas, J. L.; Logdlund, M.; Salaneck, W. R. *Nature* **1999**, *397*, 121−128.
(5) Adamovich, V.; Brooks, J.; Tamayo, A.; Alexander, A. M.; Djurovich, P. I.; D'Andrade, B. W.; Adachi, C.; Forrest, S. R.; Thompson, M. E. *New J. Chem.* **2002**, *26*, 1171−1178.
(6) D'Andrade, B. W.; Brooks, J.; Adamovich, V.; Thompson, M. E.; Forrest, S. R. *Adv. Mater.* **2002**, *14*, 1032.
(7) Ma, B. W.; Djurovich, P. I.; Garon, S.; Alleyne, B.; Thompson, M. E. *Adv. Funct. Mater.* **2006**, *16*, 2438−2446.
(8) Huang, J. S.; Li, G.; Wu, E.; Xu, Q. F.; Yang, Y. *Adv. Mater.* **2006**, *18*, 114−117.
(9) Baldo, M. A.; O'Brien, D. F.; Thompson, M. E.; Forrest, S. R. *Phys. Rev. B* **1999**, *60*, 14422−14428.
(10) Lamansky, S.; Djurovich, P.; Murphy, D.; Abdel-Razzaq, F.; Lee, H. E.; Adachi, C.; Burrows, P. E.; Forrest, S. R.; Thompson, M. E. *J. Am. Chem. Soc.* **2001**, *123*, 4304−4312.
(11) Brooks, J.; Babayan, Y.; Lamansky, S.; Djurovich, P. I.; Tsyba, I.; Bau, R.; Thompson, M. E. *Inorg. Chem.* **2002**, *41*, 3055−3066.
(12) Lamansky, S.; Djurovich, P. I.; Abdel-Razzaq, F.; Garon, S.; Murphy, D. L.; Thompson, M. E. *J. Appl. Phys.* **2002**, *92*, 1570−1575.
(13) Vaeth, K. M.; Tang, C. W. *J. Appl. Phys.* **2002**, *92*, 3447−3453.
(14) He, G. F.; Chang, S. C.; Chen, F. C.; Li, Y. F.; Yang, Y. *Appl. Phys. Lett.* **2002**, *81*, 1509−1511.
(15) Gong, X.; Ostrowski, J. C.; Moses, D.; Bazan, G. C.; Heeger, A. J. *Adv. Funct. Mater.* **2003**, *13*, 439−444.
(16) Gong, X.; Lim, S. H.; Ostrowski, J. C.; Moses, D.; Bardeen, C. J.; Bazan, G. C. *J. Appl. Phys.* **2004**, *95*, 948−953.
(17) Brunner, K.; van Dijken, A.; Borner, H.; Bastiaansen, J. J. A. M.; Kiggen, N. M. M.; Langeveld, B. M. W. *J. Am. Chem. Soc.* **2004**, *126*, 6035−6042.
(18) Suzuki, M.; Tokito, S.; Sato, F.; Igarashi, T.; Kondo, K.; Koyama, T.; Yamaguchi, T. *Appl. Phys. Lett.* **2005**, *86*.
(19) Deng, L.; Furuta, P. T.; Garon, S.; Li, J.; Kavulak, D.; Thompson, M. E.; Fréchet, J. M. J. *Chem. Mater.* **2006**, *18*, 386−395.
(20) Sandee, A. J.; Williams, C. K.; Evans, N. R.; Davies, J. E.; Boothby, C. E.; Kohler, A.; Friend, R. H.; Holmes, A. B. *J. Am. Chem. Soc.* **2004**, *126*, 7041−7048.
(21) Chen, Y. C.; Huang, G. S.; Hsiao, C. C.; Chen, S. A. *J. Am. Chem. Soc.* **2006**, *128*, 8549−8558.
(22) Sudhakar, M.; Djurovich, P. I.; Hogen-Esch, T. E.; Thompson, M. E. *J. Am. Chem. Soc.* **2003**, *125*, 7796−7797.
(23) Bates, F. S. *Science* **1991**, *251*, 898−905.
(24) Berggren, M.; Inganas, O.; Gustafsson, G.; Rasmusson, J.; Andersson, M. R.; Hjertberg, T.; Wennerstrom, O. *Nature* **1994**, *372*, 444−446.
(25) Granstrom, M.; Berggren, M.; Inganas, O.; Andersson, M. R.; Hjertberg, T.; Wennerstrom, O. *Synth. Met.* **1997**, *85*, 1193−1194.
(26) Nguyen, T. Q.; Kwong, R. C.; Thompson, M. E.; Schwartz, B. J. *Appl. Phys. Lett.* **2000**, *76*, 2454−2456.
(27) Tan, C. H.; Inigo, A. R.; Fann, W.; Wei, P. K.; Perng, G. Y.; Chen, S. A. *Org. Electron.* **2002**, *3*, 81−88.
(28) Iyengar, N. A.; Harrison, B.; Duran, R. S.; Schanze, K. S.; Reynolds, J. R. *Macromolecules* **2003**, *36*, 8978−8985.
(29) Alam, M. M.; Tonzola, C. J.; Jenekhe, S. A. *Macromolecules* **2003**, *36*, 6577−6587.
(30) Snaith, H. J.; Friend, R. H. *Thin Solid Films* **2004**, *451−52*, 567−571.
(31) Kim, J. S.; Ho, P. K. H.; Murphy, C. E.; Friend, R. H. *Macromolecules* **2004**, *37*, 2861−2871.
(32) Xia, Y. J.; Friend, R. H. *Adv. Mater.* **2006**, *18*, 1371.
(33) Kline, R. J.; McGehee, M. D. *Polym. Rev.* **2006**, *46*, 27−45.
(34) van Duren, J. K. J.; Yang, X. N.; Loos, J.; Bulle-Lieuwma, C. W. T.; Sieval, A. B.; Hummelen, J. C.; Janssen, R. A. J. *Adv. Funct. Mater.* **2004**, *14*, 425−434.
(35) Smith, A. P.; Smith, R. R.; Taylor, B. E.; Durstock, M. F. *Chem. Mater.* **2004**, *16*, 4687−4692.
(36) Babel, A.; Jenekhe, S. A. *Macromolecules* **2004**, *37*, 9835−9840.
(37) Bates, F. S.; Fredrickson, G. H. *Annu. Rev. Phys. Chem.* **1990**, *41*, 525−557.
(38) Bates, F. S.; Fredrickson, G. H. *Phys. Today* **1999**, *52*, 32−38.
(39) Matyjaszewski, K. *Chem.−A Eur. J.* **1999**, *5*, 3095−3102.
(40) Hawker, C. J.; Bosman, A. W.; Harth, E. *Chem. Rev.* **2001**, *101*, 3661−3688.
(41) Kamigaito, M.; Ando, T.; Sawamoto, M. *Chem. Record* **2004**, *4*, 159−175.
(42) Moad, G.; Rizzardo, E.; Thang, S. H. *Austr. J. Chem.* **2005**, *58*, 379−410.
(43) Burrows, P. E.; Shen, Z.; Bulovic, V.; McCarty, D. M.; Forrest, S. R.; Cronin, J. A.; Thompson, M. E. *J. Appl. Phys.* **1996**, *79*, 7991−8006.
(44) Ma, D. G.; Hummelgen, I. A.; Hu, B.; Karasz, F. E. *J. Phys. D−Appl. Phys.* **1999**, *32*, 2568−2572.
(45) Baldo, M. A.; Adachi, C.; Forrest, S. R. *Phys. Rev. B* **2000**, *62*, 10967−10977.
(46) Ma, B. W.; Djurovich, P. I.; Thompson, M. E. *Coord. Chem. Rev.* **2005**, *249*, 1501−1510.

MA0715526